


Article

# Boosting the Power-Generation Performance of Micro-Sized Al-H<sub>2</sub>O<sub>2</sub> Fuel Cells by Using Silver Nanowires as the Cathode

Heng Zhang <sup>1</sup>, Yang Yang <sup>1,2,\*</sup>, Tianyu Liu <sup>3</sup>  and Honglong Chang <sup>1,2,\*</sup>

<sup>1</sup> Ministry of Education Key Laboratory of Micro/Nano Systems for Aerospace, School of Mechanical Engineering, Northwestern Polytechnical University, Xi'an 710072, China; zhangmingxu@mail.nwpu.edu.cn

<sup>2</sup> Unmanned System Research Institute, Northwestern Polytechnical University, Xi'an 710072, China

<sup>3</sup> Department of Chemistry, Virginia Polytechnic Institute and State University, Blacksburg, VA 24061, USA; tliu23@vt.edu

\* Correspondence: yang\_yang@nwpu.edu.cn (Y.Y.); changhl@nwpu.edu.cn (H.C.); Tel.: +86-029-8849-2841 (H.C.)

Received: 13 August 2018; Accepted: 31 August 2018; Published: 3 September 2018

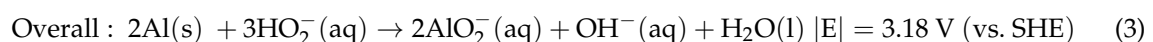
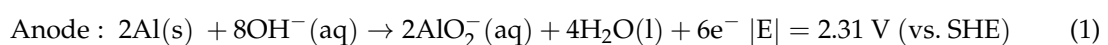


**Abstract:** Micro-sized fuel cells represent one of the pollution-free devices available to power portable electronics. However, the insufficient power output limits the possibility of micro-sized fuel cells competing with other power sources, including supercapacitors and lithium batteries. In this study, a novel aluminum-hydrogen peroxide fuel cell is fabricated using uniform silver nanowires with diameters of 0.25 μm as the catalyst at the cathode side. The Ag nanowire solution is prepared via a polyol method, and mixed uniformly with Nafion and ethanol to enhance the adhesion of Ag nanowires. We carry out electrochemical tests, including cyclic voltammetry, electrochemical impedance spectroscopy, and Tafel polarization, to characterize the performance of this catalyst in H<sub>2</sub>O<sub>2</sub> reduction. The Ag nanowires exhibit a high effectiveness and durability while catalyzing the reduction of H<sub>2</sub>O<sub>2</sub> with a low impedance. The micro-sized Al-H<sub>2</sub>O<sub>2</sub> fuel cell equipped with Ag nanowires delivers a power density of 43 W·m<sup>-2</sup> under a low concentration of H<sub>2</sub>O<sub>2</sub> (0.1 M), which is substantially higher than the previously reported devices.

**Keywords:** micro-sized fuel cells; hydrogen peroxide; catalysts; silver nanowires

## 1. Introduction

The micro power sources based on aluminum–hydrogen peroxide fuel cells (Al-H<sub>2</sub>O<sub>2</sub> FCs) have drawn increased attention due to their high theoretical open-circuit potential, high power density, and good durability [1–3]. The direct conversion of chemical energy stored in the fuels into electricity, and the H<sub>2</sub>O<sub>2</sub> reactant, make Al-H<sub>2</sub>O<sub>2</sub> FCs particularly suitable for submarine applications, where oxygen is hardly available [4–6]. Furthermore, the Al-H<sub>2</sub>O<sub>2</sub> FCs possess other advantages, including environmental friendliness, low costs, and safety [7,8]. These characteristics highlight the great potential of Al-H<sub>2</sub>O<sub>2</sub> FCs toward commercialization. The theoretical half-cell and overall chemical reactions pertaining to the Al-H<sub>2</sub>O<sub>2</sub> FCs are as follows [9]:



However, the practical energy density of Al-H<sub>2</sub>O<sub>2</sub> FCs was still insufficient for powering practical micro-sized devices, due to their limited H<sub>2</sub>O<sub>2</sub> catalytic area, poor activity of H<sub>2</sub>O<sub>2</sub> catalyzation, self-decomposition reactions of hydrogen peroxide, as well as aluminum corrosion [9]. Among the above limitations, the cathode performance related to the H<sub>2</sub>O<sub>2</sub> catalyzation plays a vital role in determining the overall fuel cell performance [10–12]. Extensive studies have been carried out in exploring suitable cathode catalysts and architectures for catalyzing H<sub>2</sub>O<sub>2</sub> reduction reactions. Patrisi et al. employed a textile flocking technique to fabricate a microfiber carbon electrode coated by a layer of alloy of Pd and Ir as the cathode [13]. Yang et al. synthesized nano-island-shaped silver particles [2]. The cathode material was achieved by electrodepositing the metallic Ag catalyst on a Ni-foam substrate. Even though Al-H<sub>2</sub>O<sub>2</sub> fuel cells equipped with these cathodes exhibited high power densities, the techniques and materials demonstrated in these works were typically expensive and time-consuming.

Here, silver nanowires (Ag NWs) were synthesized and utilized for the first time as the hydrogen peroxide reduction reaction catalyst. The morphology and structure of the Ag NWs coated on carbon paper (denoted as Ag NW//CC hereafter) were characterized using scanning electron microscope (SEM) and energy dispersive X-ray spectroscopy (EDS). Electrochemical testing methods, including cyclic voltammetry (CV), electrochemical impedance spectroscopy (EIS), and Tafel polarization curve, were carried out to investigate its catalytic activity and stability. Finally, we designed and fabricated a microfluidic Al-H<sub>2</sub>O<sub>2</sub> FC, and characterized its power-generation performance.

## 2. Results and Discussions

### 2.1. Characterization of Electrode Surface

The morphologies of Ag NW//CC were firstly characterized by SEM. As shown in Figure 1a, it could be seen that the carbon paper (CC) was made of carbon fibers with diameters of approximately 10  $\mu\text{m}$ . Upon coating with Ag NW, the surface of CC was homogeneously covered with multilayered Ag NWs (Figure 1b). The diameter and the length of the Ag NWs were approximately 0.25  $\mu\text{m}$  and 40  $\mu\text{m}$ , respectively. The Ag NWs coated on CC could increase the specific catalytic surface area, as well as enhance the mass transport kinetics [2].

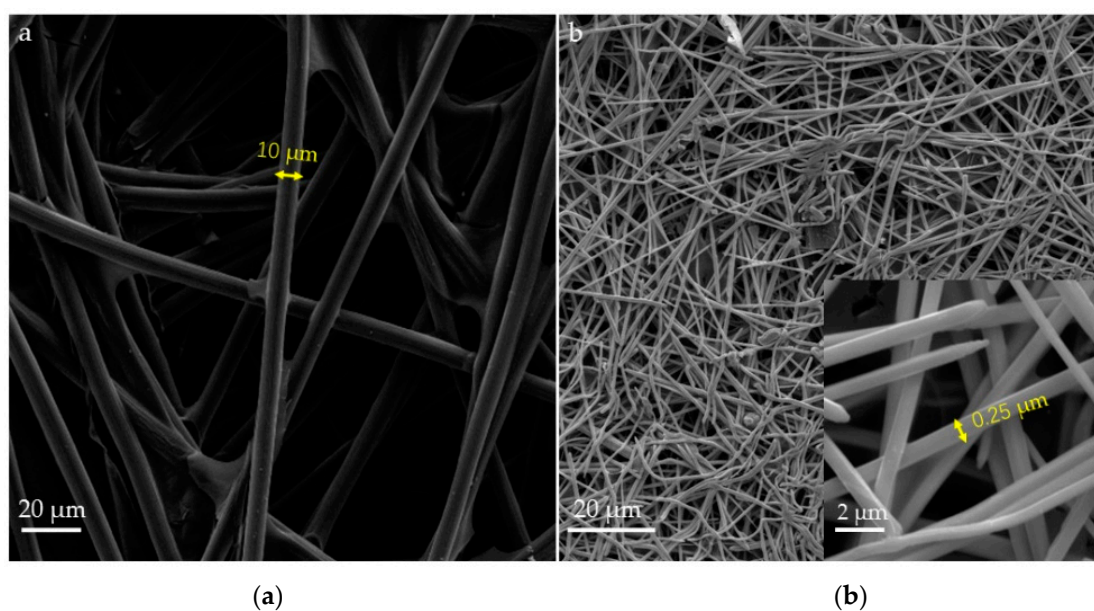


**Figure 1.** Scanning electron microscope (SEM) image of carbon paper (CC) (a) and silver nanowire (Ag NW)//CC (b). The inset image indicates the magnified morphology of Ag NWs.

## 2.2. Ag NW//CC Electrode Performance Test

### 2.2.1. Cyclic Voltammetry Performance of the Ag NW//CC Electrode

To determine the catalytic performance of the Ag NW//CC electrode, the CV measurements of Ag NW//CC and CC electrodes were conducted in identical  $\text{H}_2\text{O}_2$  electrolyte. The areas of both CC and Ag NW//CC were  $1\text{ cm} \times 1\text{ cm}$ , and the weight of Ag NW//CC and CC were 0.007 g and 0.012 g, respectively, indicating the mass loading of the silver nanowires was  $5\text{ mg}\cdot\text{cm}^{-2}$ . As shown in Figure 2, the waveforms were consistent with the previous studies reported by Honda et al. [14,15]. The oxidation peak and the reduction peak are of a similar area size, which can be ascribed to the following redox reaction:



The small oxidation and corresponding reduction peaks are attributed to the following redox reaction:

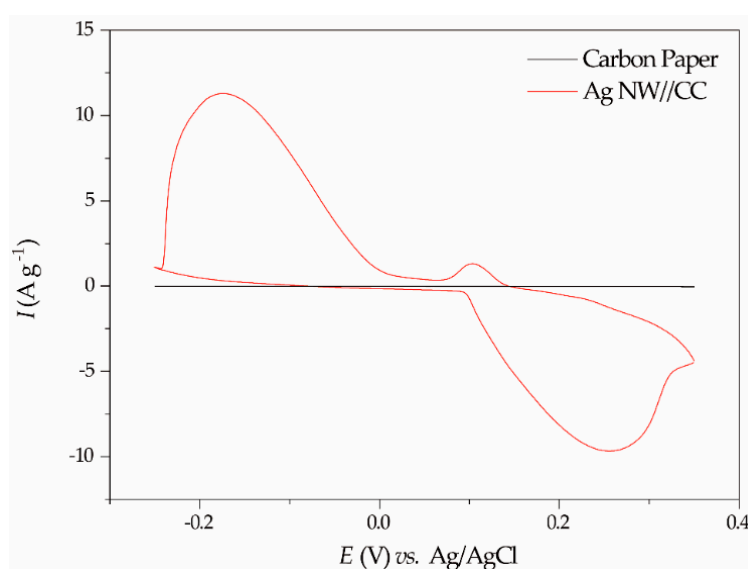


**Figure 2.** Cyclic voltammetry (CV) curves of pristine CC and Ag NW//CC electrodes. The current was calculated based on the normalization to the electrode weight.

As shown in Figure 2, the CV curve of CC was almost a straight line with marginal enclosed area, indicating there was no reaction occurring at the surface of the pristine CC. Comparably, Ag NW//CC exhibited an obvious oxidation and reduction peaks with the onset potential and current value of approximately  $-0.25\text{ V}$  and  $12\text{ A}\cdot\text{g}^{-1}$ , respectively. The positions of the reduction and oxidation peaks were in agreement with the previous reports, which indicated that Ag NW//CC could effectively catalyze the  $\text{H}_2\text{O}_2$  reduction reaction (Reaction (2)) [14,15].

To further determine the long-term catalytic durability of Ag NW//CC, 50 cycles of CV measurements were conducted on the Ag NW//CC electrode. Figure 3 showed the stability performance of Ag NW//CC in  $\text{H}_2\text{O}_2$  electrolyte. During the cycled test, the peak intensity of CV curves was well retained, but the peak position of Ag NW//CC shifted slightly under different cycles. This observation indicates that the Ag NW//CC electrode underwent certain changes during the long-term stability tests. Based on the EDS analysis (Tables S1 and S2 in the Supplementary Materials), we believe the change was the emergence of  $\text{Ag}_2\text{O}$  particles onto the Ag NWs.

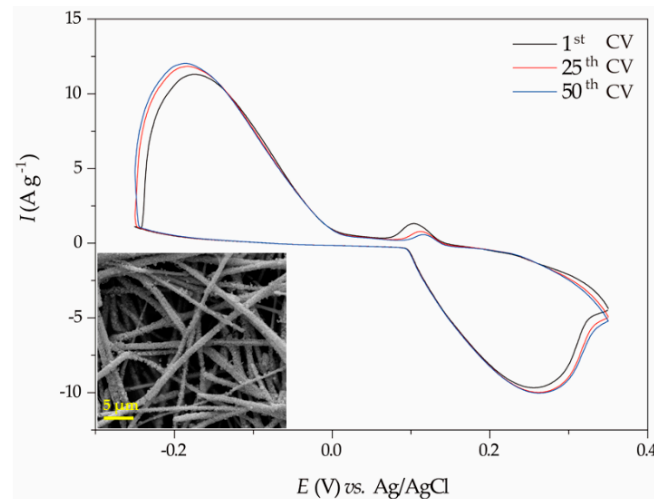


**Figure 3.** CV plots of scanning cycles of 1, 25, and 50. The inset SEM image exhibits the morphology of Ag NWs after the CV scanning.

### 2.2.2. Tafel Polarization of the Ag NW//CC Electrode

The reaction kinetics of the samples were further studied using the Tafel polarization curves (Figure 4). The fluctuation of the CC curve is because of the decomposition of hydrogen peroxide that evolves gas bubbles [16–19]. In the Tafel plot, the value of exchange current density ( $j_0$ ) can be obtained from Tafel equation (Equation (6)) according to the intercept of  $y$ -axis:

$$\log |j| = \log j_0 + \left( \frac{\beta n F}{2.303 R T} \right) |\eta| \quad (6)$$

where  $j$  is the measured current density,  $j_0$  is exchange current density,  $\beta$  is electron transfer coefficient for reductive reaction,  $n$  is number of electrons transferred,  $F$  is Faraday's constant,  $R$  is gas constant,  $T$  is temperature, and  $\eta$  is overpotential. Exchange current is the current density of working electrode when overpotential is zero. It relates to the electrochemical activity of the electrode at equilibrium state.  $j_0$  was calculated according to the Tafel equation (Equation (6)) using the data in the linear region. As shown in the figure, the  $j_0$  of the Ag NW//CC electrode is considerably boosted compared to the value of the pristine CC electrode. The enhanced current density can be attributed to the effective catalytic activity because of the presence of silver catalysts.

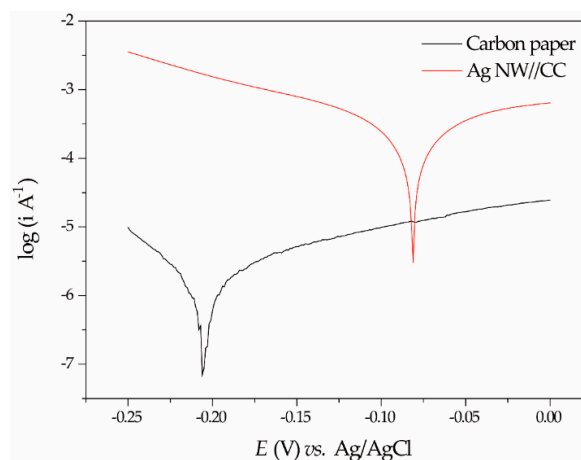


**Figure 4.** Tafel polarization curve of pristine CC and Ag NW//CC.

### 2.2.3. Characterization of Electrode Resistance

To determine the impedance of the electrode, EIS electrochemical tests were carried out from 100 kHz to 0.1 Hz. As shown in Figure 5, the semicircles in the two cases in the high frequency region were related to the charge transfer process [20]. The value of the diameters of the semicircles on the real axis are usually used to estimate the value of charge transfer resistance ( $R_{ct}$ ) [20]. Based on the calculation,  $R_{ct}$  of the electrode was tremendously decreased by more than 10 times after growing Ag NWs on the CC electrode. With respect to the curve in the low frequency region, it could be attributed to the Warburg impedance ( $R_{\Omega}$ ). The value of  $R_{\Omega}$  was typically related to the resistance of ion diffusion in the electrode materials as well as the mass transfer in electrolyte [21]. It can be estimated according to the value of last point in the Nyquist curve [21]. As indicated in Figure 5, the mass transfer resistance of the Ag NW//CC electrode was much lower than the pristine CC electrode. The EIS result is in good agreement with the CV results, indicating our Ag NW//CC electrode has a superior catalytic behavior.

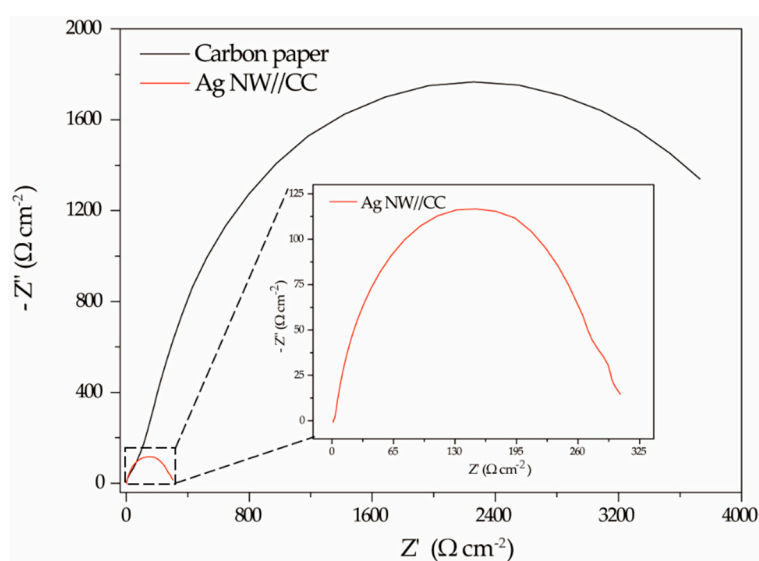


**Figure 5.** Electrochemical impedance spectroscopy (EIS) curves of pristine CC and Ag NW//CC electrodes. Inset is the magnified EIS curve of the Ag NW//CC electrode.

### 2.3. Cell Performance Test of the Micro-Sized Al-H<sub>2</sub>O<sub>2</sub> FC

Microfluidic Al-H<sub>2</sub>O<sub>2</sub> FC was fabricated using Al as anode and Ag NW//CC as cathode, and its overall performance was tested at room temperature serving the 0.1 M H<sub>2</sub>O<sub>2</sub>, 1 M NaOH and 20 g·L<sup>-1</sup> as electrolyte. As Figure 6 shows, the microfluidic Al-H<sub>2</sub>O<sub>2</sub> FC delivered an open circuit potential (OCP) of 1.55 V, which was lower than the theoretical voltage (3.18 V). This may be due to the contact resistance occurred at the electrode/substrate interface, and the mixed potential at the interface resulting from the direct oxidation of H<sub>2</sub>O<sub>2</sub> to H<sub>2</sub>O and O<sub>2</sub> [22]. The device delivered a maximum power density of 43 W·m<sup>-2</sup> at a voltage of 0.7 V. The cell performance was substantially higher than those of other Al-H<sub>2</sub>O<sub>2</sub> FCs employing other materials as cathode, and comparable to other state-of-art microfluidic fuel cells (Table 1). Significantly, the cell performance was realized by utilizing the low concentration of reactant (0.1 M), and worked at the room temperature (20 °C).

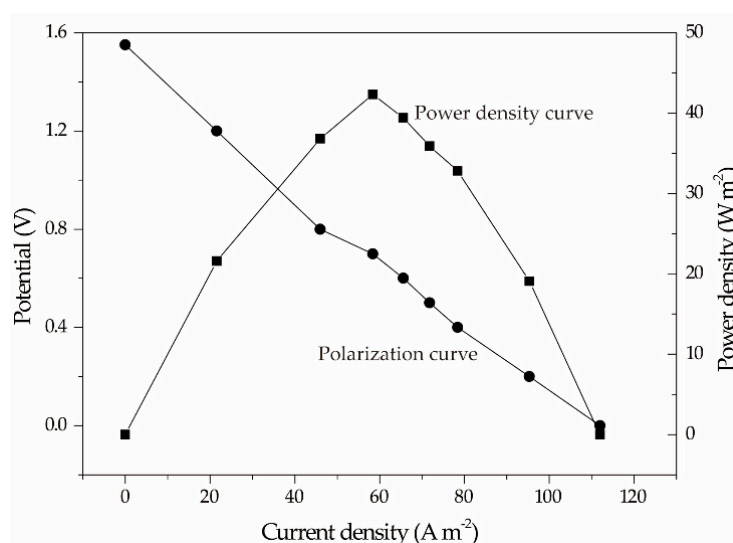


**Figure 6.** The polarization and power-density curves of the Al-H<sub>2</sub>O<sub>2</sub> FC utilizing the Ag NW//CC cathode.

**Table 1.** Performance comparison of this work with selected micro-sized fuel cells reported in the literatures.

Anode Catalyst	Cathode Catalyst	Electrolyte	$I_{\max\text{-areal}}$ (A·m <sup>-2</sup> )	$P_{\max\text{-areal}}$ (W·m <sup>-2</sup> )	Ref.
aluminum	Ag NW	0.1 M H <sub>2</sub> O <sub>2</sub> & 1 M NaOH & 20 g·L <sup>-1</sup> NaCl	112	43	This work
silver	Prussian blue	0.1 M HCl & 0.5 M H <sub>2</sub> O <sub>2</sub>	57 <sup>a</sup>	8 <sup>b</sup>	[8]
nickel	Prussian blue	0.1 M HCl & 0.5 M H <sub>2</sub> O <sub>2</sub>	101 <sup>a</sup>	15 <sup>b</sup>	[8]
Ni/carbon nanotube sponge	Pt/C	Anolyte: 3 M urea in 3 M KOH; catholyte: 1.5 M H <sub>2</sub> SO <sub>4</sub>	230 <sup>b</sup>	39 <sup>b</sup>	[23]
Pt-Ru/C	Pt <sub>x</sub> Se <sub>y</sub> /C (x/y = 5:1)	5 M methanol & 0.5 M H <sub>2</sub> SO <sub>4</sub>	409 <sup>a</sup>	30 <sup>a</sup>	[24]
aluminum	Prussian blue	0.1 M HCl & 0.5 M H <sub>2</sub> O <sub>2</sub>	45 <sup>a</sup>	10 <sup>b</sup>	[11]
Pt-Ru on Au COP	Pt/CC (40 wt %)	4 M methanol & 1 M NaOH	155 <sup>a</sup>	32 <sup>a</sup>	[25]
Au-Ag/C	Vulcan XC-72	Laccase/glucose	19 <sup>a</sup>	5 <sup>b</sup>	[26]
Pt	carbon nitride nanofibers	Anolyte: 2.1 M HCOOH catholyte: 0.144 M KMnO <sub>4</sub>	97 <sup>a</sup>	34 <sup>a</sup>	[27]
Pt	Pt	Anolyte: 2.1 M HCOOH catholyte: 0.144 M KMnO <sub>4</sub>	61 <sup>a</sup>	30 <sup>a</sup>	[27]
Pt	Au	Anolyte: 2.1 M HCOOH catholyte: 0.144 M KMnO <sub>4</sub>	60 <sup>a</sup>	27 <sup>a</sup>	[27]
Pt-Ru	Pt Black	3 M methanol (QN3 designation)	260 <sup>b</sup>	39 <sup>a</sup>	[28]

<sup>a</sup> values calculated based on the reported data; <sup>b</sup> values estimated from the reported figures.

### 3. Materials and Methods

All chemicals were reagent grade quality and obtained from the supplier without further purification. All solutions were prepared using deionized (DI) water.

#### 3.1. Synthesis and Purification of Ag NW Solution

Ag NWs were prepared through a modified polyol process [29,30]. Briefly, 100 mL ethylene glycol (EG) containing 0.19 M polyvinylpyrrolidone (PVP, molecular weight = 50 kDa), 0.05 mM NaCl, 0.0014 mM AgNO<sub>3</sub> and 0.017 mM CuCl<sub>2</sub> was added to a round-bottom flask. The flask was preheated at 185 °C in an oil bath for 1 h, while 30 mL EG solution containing 0.12 M AgNO<sub>3</sub> was prepared. The EG solution was sonicated and then added drop-wise into the flask, following the 1 h pre-heating treatment. The injection rate was precisely controlled to 0.5 mL·min<sup>-1</sup>, and vigorously stirred while



injecting. After injection, the whole flask was heated for 20 min before being removed from the oil bath, and then cooled down to room temperature.

Silver nanoparticles were observed as impurities during the polyol synthesis process of Ag NWs [31]. To purify the Ag NWs, the as-prepared solution was first diluted by deionized water to ~500 mL, then left still for 24 h to let NWs settle to the bottom. The supernatant was then carefully removed by a syringe, and deionized water was refilled to the original volume. The mixture was left still again for another sedimentation. When removing supernatant for the second time, we mixed the remaining solution with acetone at a ratio of 1:4, and vortexed the mixture thoroughly. Next, the mixture was centrifuged at the speed of 2000 rpm for 10 min, and the supernatant was decanted carefully and then a small amount of DI water was added. Acetone was added again, and the centrifuging process repeated. The whole purification procedure was repeated for 3–4 times until the silver particles were removed [32,33].

### 3.2. Electrode Synthesis

The Ag NW//CC electrode was fabricated by a homemade method. Specifically, the as-made Ag NW solution, Nafion solution, and ethanol were mixed at the ratio of 9:4:1, and subject to ultrasonic treatment to make the mixture uniform. The mixture was sprayed onto the CC electrode, and then the synthesized Ag NW//CC electrode was left to dry in air for 2 h to obtain the Ag NW//CC electrode.

### 3.3. Analysis of Electrode

The surface morphology of CC and Ag NW//CC were characterized by employing VEGA 3 LMU scanning electron microscope. The CV measurements, Tafel polarization, and EIS tests were carried out by employing an electrochemical workstation (CHI 660E, CH Instruments, Inc. Shanghai, China) in a homemade three-electrode electrochemical cell consisting of an Ag NW//CC electrode (geometric area 1 cm × 1 cm) as the working electrode, a platinum wire as a counter electrode, and an Ag/AgCl (in saturated KCl solution) electrode as the reference electrode [34].

The electrolyte was composed of 0.1 M H<sub>2</sub>O<sub>2</sub>, 1.0 M NaOH, and 20 g·L<sup>-1</sup> NaCl solution. The low concentration of H<sub>2</sub>O<sub>2</sub> and NaOH was chosen according to previous research to reduce the self-decomposition reaction of H<sub>2</sub>O<sub>2</sub> to ensure the safety of the operation [14]. CV measurements were carried out from -0.25 V to 0.35 V at a rate of 10 mV·s<sup>-1</sup> at 20 °C. EIS tests were carried out from 10 kHz to 0.1 Hz.

### 3.4. Fuel Cell Set-Up

The schematic of micro-sized Al-H<sub>2</sub>O<sub>2</sub> FC was illustrated in Figure 7. The Al plate with the size of 30 mm × 20 mm × 0.3 mm served both as the electrode and baseplate. A chamber of 10 mm × 10 mm × 5 mm was grooved on the base of poly (methylmethacrylate) (PMMA) by employing a numerically controlled machine, and plated on the surface of Al plate. The inlet and outlet were drilled on the top of chamber with a diameter of 1.0 mm, and then the Ag NW//CC cathode, together with a copper plate, was mounted on the PMMA. The copper plate was employed as a current collector of Ag NW//CC cathode. The whole system was compacted tightly by a parallel-jaw vice and two PMMA plates. The electrolyte was pumped into the fuel cell system at the flow rate of 0.5 mL·min<sup>-1</sup>.

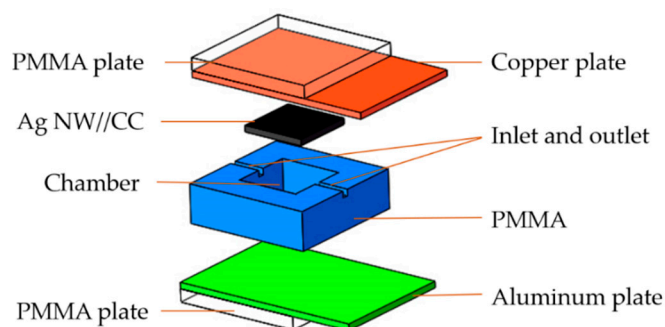


**Figure 7.** Schematic of the microfluidic Al-H<sub>2</sub>O<sub>2</sub> FC equipped with Ag NW//CC cathode.

#### 4. Conclusions

In this work, a novel H<sub>2</sub>O<sub>2</sub> reduction reaction catalyst was prepared by anchoring silver nanowires on carbon fibers via a simple approach. The SEM images and EDS analysis of Ag NW//CC demonstrated the multilayers of silver nanowires were grown firmly on CC. CV measurements revealed that Ag NW//CC had an excellent catalytic efficiency and good stability towards the H<sub>2</sub>O<sub>2</sub> reduction reaction. The Ag NW//CC had a superior performance in terms of the electrode impedance. The micro-sized Al-H<sub>2</sub>O<sub>2</sub> FC delivered a power density of 43 W·m<sup>-2</sup> with a maximum current density of 112 A·m<sup>-2</sup>. These features make Ag NW//CC a promising candidate for catalyzing the H<sub>2</sub>O<sub>2</sub> reduction reaction, and a suitable electrode for aluminum-hydrogen peroxide fuel cells.

**Supplementary Materials:** The supplementary materials are available online at <http://www.mdpi.com/1996-1073/11/9/2316/s1>, Tables S1 and S2: Element analysis of Ag NWs before and after the stability test.

**Author Contributions:** H.Z. did the experiments, analyzed the data and drafted the manuscript. Y.Y. guided the electrochemical experiments and supervised the work. T.L. and H.C. revised the manuscript. T.L. motivated the research.

**Funding:** This research was funded by the National Natural Science Foundation of China (No. 51706184), the key laboratory of low-grade energy utilization technologies and system (No. LLEUTS-201813), and the Fundamental Research Funds for the Central Universities (No. 3102017OQD011).

**Acknowledgments:** The authors acknowledge the financial support from the funding agencies listed above. Tianyu Liu expresses gratitude for the support from Chinese Government Award for Outstanding Self-Financed Students Abroad.

**Conflicts of Interest:** The authors declare no conflict of interest.

#### References

- Bahrebar, S.; Blaabjerg, F.; Wang, H.; Vafamand, N.; Khooban, M.-H.; Rastayesh, S.; Zhou, D. A novel type-2 fuzzy logic for improved risk analysis of proton exchange membrane fuel cells in marine power systems application. *Energies* **2018**, *11*, 721. [[CrossRef](#)]
- Yang, W.; Yang, S.; Sun, W.; Sun, G.; Xin, Q. Nanostructured silver catalyzed nickel foam cathode for an aluminum–hydrogen peroxide fuel cell. *J. Power Source* **2006**, *160*, 1424. [[CrossRef](#)]
- Dow, E.G.; Bessette, R.R.; Seebach, G.L.; Marsh-Orndorff, C.; Meunier, H.; VanZee, J.; Medeiros, M.G. Enhanced electrochemical performance in the development of the aluminum/hydrogen peroxide semi-fuel cell. *J. Power Sources* **1997**, *65*, 207–212. [[CrossRef](#)]
- Deuchars, G.D.; Hill, J.R.; Stannard, J.H.; Stockburger, D.C. Aluminum-hydrogen peroxide power system for an unmanned underwater vehicle. *Oceans* **1993**, *152*, 158–165.
- Mendez, A.; Leo, T.; Herreros, M. Current state of technology of fuel cell power systems for autonomous underwater vehicles. *Energies* **2014**, *7*, 4676–4693. [[CrossRef](#)]
- Luo, N.; Miley, G.H.; Gimlin, R.J.; Burton, R.L.; Rusek, J.; Holcomb, F. Hydrogen-peroxide-based fuel cells for space power systems. *J. Propul. Power* **2012**, *24*, 583–589. [[CrossRef](#)]
- Debe, M.K. Electrocatalyst approaches and challenges for automotive fuel cells. *Nature* **2012**, *486*, 43–51. [[CrossRef](#)] [[PubMed](#)]



8. Mousavi Shaegh, S.A.; Nguyen, N.-T.; Mousavi Ehteshami, S.M.; Chan, S.H. A membraneless hydrogen peroxide fuel cell using prussian blue as cathode material. *Energy Environ. Sci.* **2012**, *5*, 8225. [[CrossRef](#)]
9. Brodrecht, D.J.; Rusek, J.J. Aluminum–hydrogen peroxide fuel-cell studies. *Appl. Energy* **2003**, *74*, 113–124. [[CrossRef](#)]
10. Bessette, R.R.; Cichon, J.M.; Dischert, D.W.; Dow, E.G. A study of cathode catalysis for the aluminium/hydrogen peroxide semi-fuel cell. *J. Power Sources* **1999**, *80*, 248–253. [[CrossRef](#)]
11. Asadnia, M.; Mousavi Ehteshami, S.M.; Chan, S.H.; Warkiani, M.E. Development of a fiber-based membraneless hydrogen peroxide fuel cell. *RSC Adv.* **2017**, *7*, 40755–40760. [[CrossRef](#)]
12. Marsh, C.L.; Seebach, G.L.; Vanzee, J.W.; Bessette, R.R.; Meunier, H.G. Preparation of an electrocatalytic cathode for an aluminum-hydrogen peroxide battery. U.S. Patent No. 5,296,429, 22 March 1994.
13. Patrissi, C.; Bessette, R.R.; Kim, Y.; Schumacher, R.C. Fabrication and rate performance of a microfiber cathode in a mg–H<sub>2</sub>O<sub>2</sub> flowing electrolyte semi-fuel cell. *J. Electrochem. Soc.* **2008**, *155*, B558–B562. [[CrossRef](#)]
14. Honda, M.; Kodera, T.; Kita, H. On the electrochemical behavior of H<sub>2</sub>O<sub>2</sub> at ag in alkaline solution. *Electrochim. Acta* **1983**, *28*, 727–733. [[CrossRef](#)]
15. Tilak, B.V.; Perkins, R.S.; Kozłowska, H.A.; Conway, B.E. Impedance and formation characteristics of electrolytically generated silver oxides—Formation and reduction of surface oxides and the role of dissolution processes. *Electrochim. Acta* **1972**, *17*, 1447–1469. [[CrossRef](#)]
16. Shu, C.; Wang, E.; Jiang, L.; Tang, Q.; Sun, G. Studies on palladium coated titanium foams cathode for mg–H<sub>2</sub>O<sub>2</sub> fuel cells. *J. Power Sources* **2012**, *208*, 159–164. [[CrossRef](#)]
17. Lue, S.; Liu, N.-Y.; Rajesh Kumar, S.; Tseng, K.; Wang, B.-Y.; Leung, C.-H. Experimental and one-dimensional mathematical modeling of different operating parameters in direct formic acid fuel cells. *Energies* **2017**, *10*, 1972. [[CrossRef](#)]
18. Oliveira, F.M.D.; Guedes, T.D.J.; Lima, A.B.; Silva, L.M.D.; Santos, W.T.P.D. Alternative method to obtain the tafel plot for simple electrode reactions using batch injection analysis coupled with multiple-pulse amperometric detection. *Electrochim. Acta* **2017**, *242*, 180–186. [[CrossRef](#)]
19. Sharma, S.; Zhang, K.; Gupta, G.; Santamaria, D. Exploring pani-tin nanoparticle coatings in a pefc environment: Enhancing corrosion resistance and conductivity of stainless steel bipolar plates. *Energies* **2017**, *10*, 1152. [[CrossRef](#)]
20. Hu, C.; Xiao, Y.; Zhao, Y.; Chen, N.; Zhang, Z.; Cao, M.; Qu, L. Highly nitrogen-doped carbon capsules: Scalable preparation and high-performance applications in fuel cells and lithium ion batteries. *Nanoscale* **2013**, *5*, 2726–2733. [[CrossRef](#)] [[PubMed](#)]
21. Barsoukov, E.; Macdonald, J.R. Impedance spectroscopy: Theory, experiment, and applications. *J. Hosp. Palliat. Nurs.* **2005**, *4*, 206–207.
22. León, C.P.D.; Walsh, F.C.; Rose, A.; Lakeman, J.B.; Browning, D.J.; Reeve, R.W. A direct borohydride–acid peroxide fuel cell. *J. Power Sources* **2007**, *164*, 441–448. [[CrossRef](#)]
23. Zhang, H.; Wang, Y.; Wu, Z.; Leung, D.Y.C. A direct urea microfluidic fuel cell with flow-through ni-supported-carbon- nanotube-coated sponge as porous electrode. *J. Power Sources* **2017**, *363*, 61–69. [[CrossRef](#)]
24. Ma, J.; Habrioux, A.; Morais, C.; Alonso-Vante, N. Electronic modification of Pt via Ti and Se as tolerant cathodes in air-breathing methanol microfluidic fuel cells. *Phys. Chem. Chem. Phys.* **2014**, *16*, 13820–13826. [[CrossRef](#)] [[PubMed](#)]
25. Esquivel, J.P.; Del Campo, F.J.; Gómez de la Fuente, J.L.; Rojas, S.; Sabaté, N. Microfluidic fuel cells on paper: Meeting the power needs of next generation lateral flow devices. *Energy Environ. Sci.* **2014**, *7*, 1744–1749. [[CrossRef](#)]
26. López-González, I.B.; Dector, A.; Cuevas-Muñiz, F.M.; Arjona, N.; Cruz-Madrid, C.; Arana-Cuenca, A.; Guerra-Balcázar, z.M.; Arriaga, L.G.; Ledesma-García A, J. Hybrid microfluidic fuel cell based on laccase/c and auag/c electrodes. *Biosens. Bioelectron.* **2014**, *62*, 221–226. [[CrossRef](#)] [[PubMed](#)]
27. Jindal, A.; Basu, S.; Chauhan, N.; Ukai, T.; Kumar, D.S.; Samudhyatha, K.T. Application of electrospun cnx nanofibers as cathode in microfluidic fuel cell. *J. Power Sources* **2017**, *342*, 165–174. [[CrossRef](#)]
28. Falcão, D.; Silva, R.; Rangel, C.; Pinto, A. Performance of an Active Micro Direct Methanol Fuel Cell Using Reduced Catalyst Loading MEAs. *Energies* **2017**, *10*, 1683. [[CrossRef](#)]
29. Sun, Y.; Gates, B.; Brian Mayers, A.; Xia, Y. Crystalline silver nanowires by soft solution processing. *Nano Lett.* **2002**, *2*, 165–168. [[CrossRef](#)]

30. Sun, Y.; Yin, Y.; Mayers, B.T.; Herricks, T.; Xia, Y. Uniform silver nanowires synthesis by reducing AgNO<sub>3</sub> with ethylene glycol in the presence of seeds and poly(vinyl pyrrolidone). *Chem. Mater.* **2002**, *14*, 4736–4745.
31. Coskun, S.; Aksoy, B.; Unalan, H.E. Polyol synthesis of silver nanowires: An extensive parametric study. *Cryst. Growth Des.* **2011**, *11*, 4963–4969. [[CrossRef](#)]
32. Li, B.; Ye, S.; Stewart, I.E.; Alvarez, S.; Wiley, B.J. Synthesis and purification of silver nanowires to make conducting films with a transmittance of 99%. *Nano Lett.* **2015**, *15*, 6722. [[CrossRef](#)] [[PubMed](#)]
33. Mayousse, C.; Celle, C.; Moreau, E.; Mainguet, J.F.; Carella, A.; Simonato, J.P. Improvements in purification of silver nanowires by decantation and fabrication of flexible transparent electrodes: Application to capacitive touch sensors. *Nanotechnology* **2013**, *24*, 215501. [[CrossRef](#)] [[PubMed](#)]
34. Fu, Q.; Xiao, S.; Li, Z.; Li, Y.B.; Kobayashi, H.; Li, J.; Yang, Y.; Liao, Q.; Zhu, X.; He, X.F.; et al. Hybrid solar-to-methane conversion system with a Faradaic efficiency of up to 96%. *Nano Energy* **2018**, *53*, 232–239. [[CrossRef](#)]



© 2018 by the authors. Licensee MDPI, Basel, Switzerland. This article is an open access article distributed under the terms and conditions of the Creative Commons Attribution (CC BY) license (<http://creativecommons.org/licenses/by/4.0/>).